PHYSICAL REVIEW B **77**, 064424 (2008)

Griffiths phase and critical behavior in single-crystal $La_{0.7}Ba_{0.3}MnO_3$: Phase diagram for $La_{1-x}Ba_xMnO_3$ ($x \leqslant 0.33$)

Wanjun Jiang,[*] XueZhi Zhou, and Gwyn Williams
Department of Physics and Astronomy, University of Manitoba, Winnipeg, Manitoba R3T 2N2, Canada

Y. Mukovskii and K. Glazyrin
Moscow State Steel and Alloys Institute, Moscow 119049, Russia

(Received 8 November 2007; revised manuscript received 19 December 2007; published 21 February 2008)

Analyses of temperature- and field-dependent ac susceptibility and magnetization data from a colossal magnetoresistive $La_{0.7}Ba_{0.3}MnO_3$ single crystal in terms of scaling behavior yield exponent values of $\delta = 5.5 \pm 0.3$ and $\gamma = 1.41 \pm 0.02$ (both slightly larger than Heisenberg model predictions), with $\beta = 0.35 \pm 0.04$ and a Curie temperature $T_C = 310 \pm 0.5$ K. Detailed investigation of the low-field dc and ac susceptibilities reveals features consistent with the presence of a Griffiths phase (GP)—viz., an inverse susceptibility characterized by $\chi^{-1} \propto (T - T_C^R)^{1-\lambda}$ with $\lambda = 0.67 \pm 0.05$. These, combined with previous results, enable a phase diagram summarizing the evolution of the GP with composition in this system to be constructed, and in this context, the possible importance of the variation of the acoustic spin-wave stiffness D with composition is discussed.

DOI: 10.1103/PhysRevB.77.064424 PACS number(s): 75.40.−s, 75.40.Cx, 75.47.Lx

INTRODUCTION

Doped transition-metal oxides with a perovskite structure have been extensively studied over the past several years, a result of their displaying a colossal magnetoresistance (CMR)—viz., a very large change in resistance induced by the application of a magnetic field. Such behavior is associated with the occurrence of a metal-insulator transition, the temperature of which exhibits a marked dependence on field. However, despite extensive efforts to explain the origin of CMR behavior, initially double exchange (DE),[1] and its subsequent extension to include spontaneous electronic phase separation[2] and the occurrence of a Griffiths phase[3,4] among others, the physical mechanism underlying CMR, remains controversial. In more general terms, manganese perovskites represent an interesting class of materials with an unusual combination of coupling between charge, spin, orbital, and vibrational degrees of freedom, making them an important class of strongly correlated electronic systems.[5]

These materials are characterized by the general formula $A_{1-x}B_xMnO_3$ where A is a rare-earth ion (i.e., La,Pr,...) and B is a divalent alkaline-earth cation (i.e., Ca,Ba,...), x being the doping level, the latter causing changes in the valence state of the Mn ions to maintain charge neutrality. The consequent mismatch in the ionic size of ions occupying the A (La) site leads to a distortion in the crystal structure described by a "tolerance factor" $t = \frac{\langle r_A \rangle + r_O}{\sqrt{2}(\langle r_{Mn} \rangle + r_O)}$, where r_O is the radius of the oxygen ion, while $\langle r_A \rangle$ and $\langle r_{Mn} \rangle$ are the average radii of A and Mn ions, respectively. When t is close to 1, a cubic perovskite structure is realized; as t decreases, the lattice structure transforms first to rhombohedral ($0.96 < t < 1$) and then to orthorhombic ($t < 0.96$).[5] The tolerance factor and the variance σ in the A-site radius both provide quantitative measures of the disorder in these systems.[5] Below we present a summary of magnetic and transport data on an optimally doped $La_{0.7}Ba_{0.3}MnO_3$ single crystal, with particular emphasis on the influence of disorder which nucleates the onset of a Griffiths phase in the $La_{1-x}Ba_xMnO_3$ series of single crystals.

EXPERIMENTAL DETAILS

The single crystal used in the present study, with a nominal composition $La_{0.7}Ba_{0.3}MnO_3$, was grown using the floating zone technique.[6] It was of high structural and magnetic quality, displaying a mosaicity of less than 1° and a coercivity not exceeding 4 Oe. A Quantum Design model 6000 PPMS magnetometer-susceptometer was used to measure the field- and temperature-dependent ac susceptibility $\chi(H,T)$ (at 1 kHz with an 0.1 Oe excitation field) and the magnetization $M(H,T)$. All fields were applied along the largest sample dimension to minimize demagnetization effects. The sample composition was confirmed from the magnetization isotherm at 2 K, which yields a spontaneous magnetization of $(3.66 \pm 0.02)\mu_B/\text{Mn}$ (84.7 ± 0.3 emu/g), consistent with the theoretical spin-only value of $M_S(0) = NgS_{eff} = 3.7\mu_B/\text{Mn}$ (85.62 emu/g) calculated from the nominal composition. Magnetoresistance measurements were made using a model 7000 ac transport controller with a conventional four-probe technique and an excitation current of 0.05 mA at 499 Hz. Contacts to samples (with typical dimensions $6 \times 1 \times 1$ mm^3) were made by compressing indium "pads" over current-voltage gold-conducting wires embedded in grooves in the sample made by a diamond wire saw.

RESULTS AND DISCUSSION

Field- and temperature-dependent ac susceptibility measurements provide a powerful technique for investigating continuous magnetic phase transitions, as detailed previously,[7,8] complementing conventional techniques.[9–11] The corresponding data on the present single crystal are reproduced in Fig. 1. The inset in Fig. 1(a) shows the zero-field ac

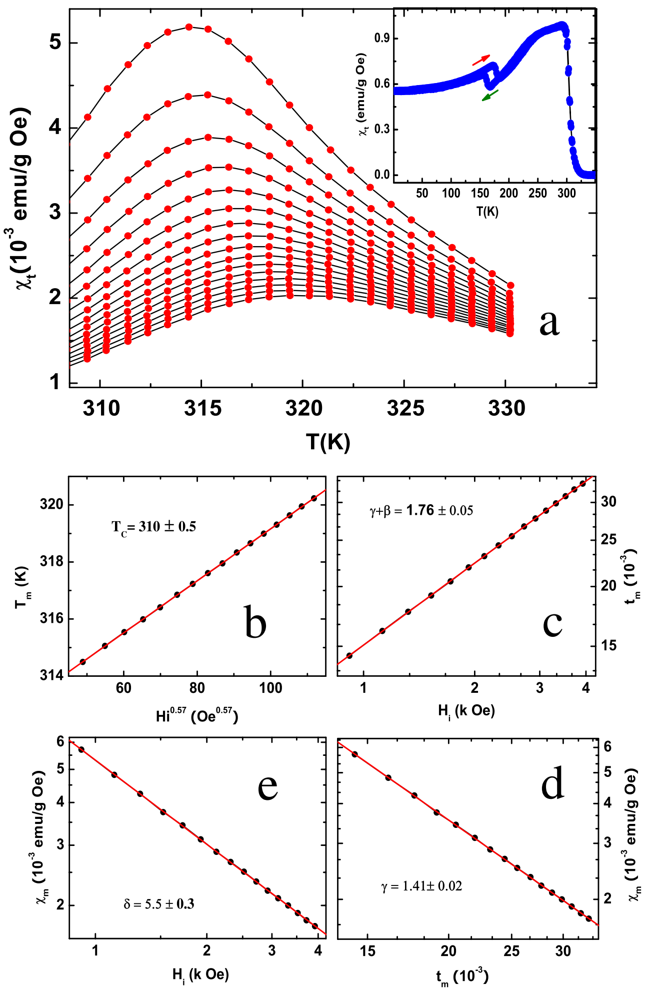

FIG. 1. (Color online) (a) Inset: the zero-field ac susceptibility, measured on warming and cooling; the main body reproduces $\chi(H,T)$ measured on warming following zero-field cooling in different static fields from 1000 Oe (top) to 4000 Oe (bottom) in 200 Oe steps; (b) estimate of critical temperature T_C by plotting the susceptibility peak temperature (T_m) against ($H_i^{0.57}$); (c), (d), (e) are double-logarithmic plots which test the various power-law predictions, Eqs. (1)–(3), these data have been corrected for background and demagnetization effects; (c) reproduces the reduced temperature (t_m), against the internal field (H_i); (d) the peak susceptibilities (χ_m) against reduced temperature (t_m); (e) the peak susceptibilities (χ_m) against internal field (H_i).

susceptibility $\chi(0,T)$ measured on warming and cooling. While there is no measurable thermal hysteresis (on a scale of typically 0.5 K) associated with the magnetic transition near 310 K, hysteresis is evident in the temperature region 157 K $<T<$ 187 K surrounding the rhombohedral $R\bar{3}c$ to orthorhombic *Pbmn* structural phase transition.[12]

The maximum susceptibility value—the Hopkinson-principal maximum[7,8]—evident in this inset yields an estimate for the demagnetization factor of $N=1/\chi_{\max}=1/0.2119=4.72$ g Oe/emu. The main body of Fig. 1(a) summarizes the field dependence of the ac susceptibility, which displays a series of peaks which decrease in amplitude $\chi(H,t_m)$ and increase in temperature (T_m) as the applied field increases. Standard critical theory indicates that the locus in temperature, t_m, and amplitude of these peaks are governed by a set of power laws[4,7,8]—viz.,

$$t_m = (T_m - T_C)/T_C \propto H_i^{(1/\gamma+\beta)}, \tag{1}$$

$$\chi_m \propto t_m^{-\gamma}, \tag{2}$$

$$\chi_m \propto H_i^{(1-\delta)/\delta}, \tag{3}$$

where H_i is the internal field ($H_i=H_a-NM$, H_a being the static applied field). The (reduced) temperature $t_m=(T-T_C)/T_C$ determines the location of the “crossover” line, above which the response is thermally dominated, as opposed to being field dominated below it.[4,7,8] Such structure is regarded as an unequivocal signature of a continuous–second-order transition (which Arrott plots—not reproduced here—confirm).

Given the success of the Heisenberg model[13] in describing the critical behavior in many manganites,[4,7–9] an attempt was made to find a quantitative estimate for T_C using the above data in conjunction with Eq. (1)—i.e., by plotting the measured peak temperatures T_m against the internal field $H_i^{0.57}$ using the Heisenberg model prediction of $(\gamma+\beta)^{-1}=0.57$ (Ref. 13) (a point returned to below). The data [Fig. 1(b)] are well represented by this form, and an extrapolation to $H_i=0$ yields an initial estimate for T_C. Typically this estimate is then used to construct double-logarithmic plots of the reduced temperature t_m against the internal field [retesting Eq. (1)] and of the peak amplitude against reduced temperature [Eq. (2)], with small adjustments to T_C until a consistent set of plots [Figs. 1(c) and 1(d)] are obtained. Such an approach confirms the corresponding power predictions and in the present sample yields $\gamma=1.41\pm0.02$ and $\beta=0.35\pm0.04$, with $T_C=310\pm0.5$ K (i.e., here the initial T_C is essentially unchanged). Notice that while the individual exponent values differ from Heisenberg model predictions, their sum (coincidentally) does not, thus validating the approach used to construct Fig. 1(b). In Fig. 1(e) the peak amplitudes from Fig. 1(a) (corrected for background and demagnetizing effects) are plotted against the internal field on a double-logarithmic scale; this figure tests the remaining power-law prediction, Eq. (3), and yields $\delta=5.5\pm0.3$ (an estimate which does not depend on choice for T_C). These estimates for γ, and δ particularly, are slightly higher than the Heisenberg model values [$\gamma=1.387$, $\beta=0.365$, $\delta=4.783$ (Ref. 13)]; however, the exponent values quoted obey the Widom relation $\gamma=\beta(\delta-1)$ (Ref. 7) within experimental uncertainty.

Confirmation of these exponent estimates is provided by the magnetization data. Figure 2(a) shows such data collected along the critical isotherm ($T_C=310$ K), with the inset in this figure evaluating δ independently using

$$M(H,T=T_C)=M_0H^{1/\delta}, \quad m(h,0)\sim Dh^{1/\delta}. \tag{4}$$

For fields comparable to those used in Fig. 1(e), this double-logarithmic plot yields $\delta=5.5\pm0.3$. Figure 2(b) demonstrates a good collapse of the magnetization data near $T_C=310$ K based on the usual scaling representation incorporating the above exponent estimates; the latter demonstrates

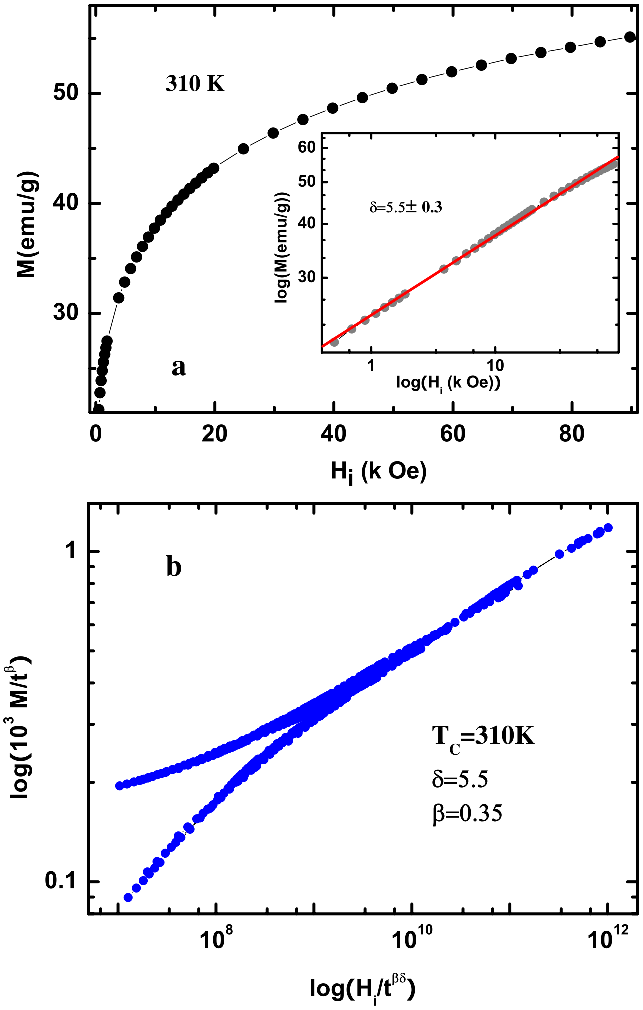

FIG. 2. (Color online) (a) Magnetization measured along the critical isotherm (T_C=310 K), the inset estimates δ by reporting the data from on a double-logarithmic scale; (b) a conventional scaling plot using the critical exponents and T_C listed above.

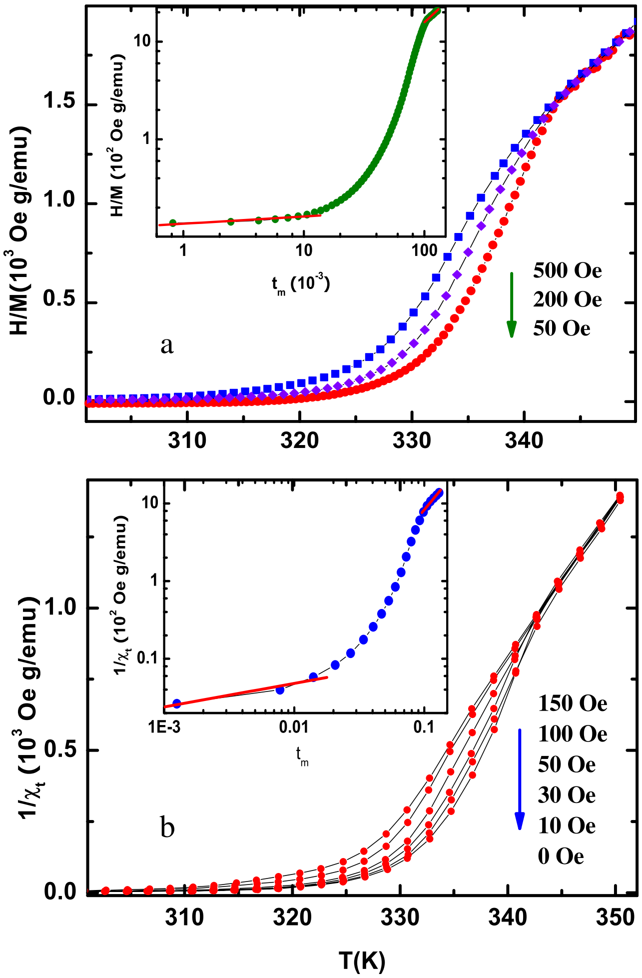

FIG. 3. (Color online) (a) The inverse dc susceptibility plotted against temperature immediately above T_C in various static fields shown; the inset, a double-logarithmic plot testing Eq. (5), yields a value of λ=0.62 (H=20 Oe) with T_C^{Rand}=310 K; (b) the corresponding inverse ac susceptibility measured in various static fields; the inset yields λ=0.67. All data were collected on warming following zero-field cooling.

convincing consistency with the ac susceptibility data.

Values of the exponent δ far in excess of the Heisenberg value have been linked with the onset of a Griffiths phase.[3,4,14–16] The characteristics of such a phase have been used successfully to reproduce CMR behavior in the LaCaMnO$_3$ system near optimal doping,[3] as well as its variation with dopant species. Griffiths phases have also been reported in the range of doped Mn perovskites and other systems based on a variety of physical measurements;[3,4,15–17] its presence reflects the influence of disorder on the phase complexity in the manganites and related systems. In the original problem treated by Griffiths,[14] nearest-neighbor exchange bonds of strength J occurred with probability p, disorder being introduced via bonds of zero strength and probability $(1-p)$. Below the percolation threshold p_c of the relevant lattice there is zero probability of establishing an infinite percolating "backbone" (in the language of continuous transitions, the correlation length does not diverge), and thus cooperative ferromagnetism is not established; neither, in the context of the manganites, is a double-exchange linked ferromagnetic pathway. By contrast, for $p > p_c$, ferromagnetic (FM) order is established, but as expected, at a temperature $T_C(p)$ below that of the undiluted system $[T_C(p=1)=T_G]$. The temperature interval $T_C(p) < T < T_G$ defines the Griffiths regime, a regime in which the system response is neither simply paramagnetic (PM) and Curie-Weiss-like nor is an infinite percolating chain and divergent correlation length established; here, the response is dominated by the largest cluster and correlated volume, leading to the following prediction[3,4,14] for the inverse susceptibility: viz.,

$$\chi^{-1} \propto (T - T_C^{Rand})^{1-\lambda}, \quad \lambda < 0 < 1. \quad (5)$$

Despite the result that the δ value in the present Ba-doped single crystal exceeds the model-predicted value to a far lesser extent than values reported in its Ca-doped counterparts,[3,4] Figs. 3(a) and 3(b), which reproduce the low-field dc and ac susceptibilities immediately above T_C, dem-

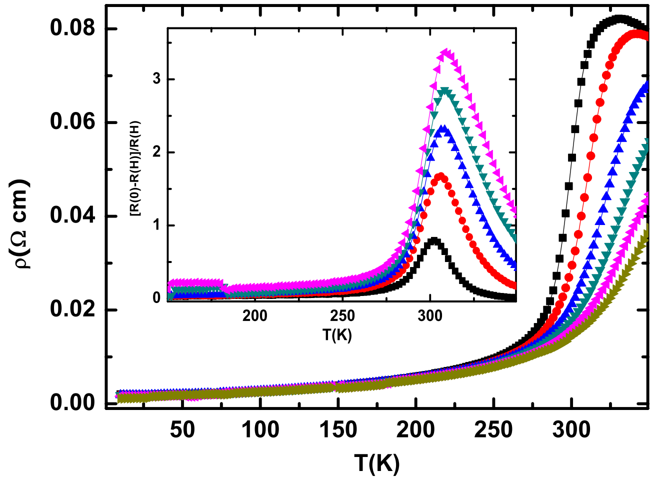

FIG. 4. (Color online) Resistivity in 0 T (top) and 1, 3, 5, 7, and 9 T (bottom) measured on warming following zero-field cooling; the inset shows the associated magnetoresistance.

onstrate clearly the depression of the inverse initial susceptibility in this temperature regime below its Curie-Weiss value, a result consistent with the formation of large correlated regions and clusters. The inset in these figures confirm the power-law prediction—Eq. (5); specifically, Fig. 3(a) utilizes a T_C^{Rand} of 310 K, a value which is consistent in this system with the Curie temperature T_C deduced from scaling analysis, with the associated fit to the 20-Oe dc data yielding $\lambda = 0.62 \pm 0.05$ $(310\ \text{K} < T < 318\ \text{K})$. The inset in Fig. 3(b) yields a consistent result, with $\lambda = 0.67 \pm 0.05$ from the zero-field ac data over the same temperature range. In the PM region $[T > T_G = 342\ \text{K}$, with T_G chosen using the same criterion as Magen *et al.*[16]—viz., the onset of the departure of the inverse susceptibility from a Curie-Weiss dependence (as higher-temperature measurements—and fits to them—are not possible in our present magnetometer)], the corresponding exponent λ is close to zero (0.011), an anticipated result as the Griffiths phase evolves into a conventionally disordered PM state. The rapid suppression of the Griffiths phase with field evident in Fig. 3 (the applied field being the conjugate field for uniform ferromagnetism rather than its disordered Griffiths counterpart) is consistent with that reported earlier for an $x = 0.27$ Ba single crystal;[17] however, the λ value deduced here, being comparable to that found in a variety of doped manganites and other systems,[3,4,17] is larger than that found at the lower composition. The latter likely reflects the result that at $x = 0.27$ the exponent values are considerably closer to Heisenberg model values. This point is returned to below.

Despite the differences in exponent values with the "regular" Griffiths phase systems,[3,4] transport measurements on the present system reveal it displays standard CMR behavior, as Fig. 4 demonstrates. The inset reproduces the associated magnetoresistance $[\rho(0) - \rho(H)]/\rho(H)$, which, as expected, exhibits a peak near the metal-insulator phase transition.

Combining the present data with our earlier results at $x = 0.27$, the recent interpretation of electron spin resonance (ESR) measurements by Eremina *et al.*,[18] and a range of previous measurements enables a modified phase diagram for the LaBaMnO$_3$ system in the vicinity of the Griffiths regime ($x \leq 0.33$) to be constructed. In particular, the present measurements demonstrate unequivocally that the conjectured termination of the Griffiths phase between $x = 0.2$ and $x = 0.3$ needs to be corrected, as Fig. 5(c) indicates; it extends to somewhat beyond $x = 0.3$, likely to optimal doping.[17,19–24] Differences in the absolute values for T_G, T_C, and x notwithstanding, Fig. 5(c) is strikingly similar to a corresponding phase diagram determined for the LaSrMnO$_3$ system,[15] which, in turn, was compared with the (T-p) diagrams for Griffiths' original diluted FM Ising model[14] and that conjectured for its $= \pm J$ random bond counterpart [Figs. 5(a) and 5(b)].

Despite the overall agreement in mapping the compositional boundaries of the Griffiths phase in this Ba-substituted system using data from several experimental techniques, some fundamental questions remain. These include both the origin of the rapid suppression of Griffiths characteristics by field in this system and the associated variation of the expo-

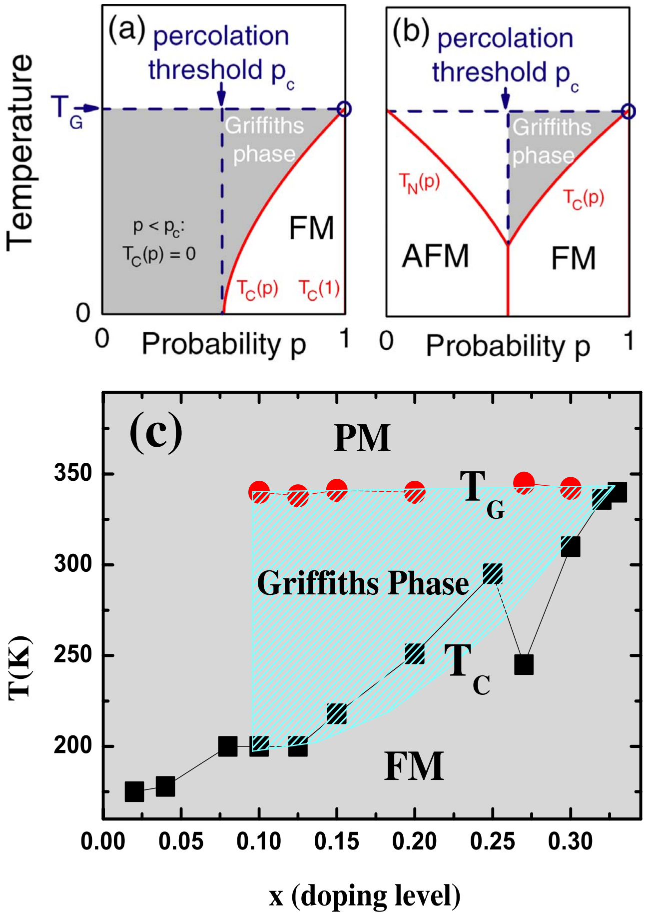

FIG. 5. (Color online) (a) The T_G-T_C-p diagram for the bond-diluted FM Ising model (Refs. 14 and 15); (b) its conjectured $\pm J$ random bond Ising model counterpart; (c) a summary of the current and prior observation of Griffiths phase boundaries for the La$_{1-x}$Ba$_x$MnO$_3$ system ($x \leq 0.33$; see text). Data in the range of $0.1 < x$ cited from Ref. 19, $0.1 < x < 0.2$ from Ref. 18, part of $0.1 < x < 0.2$ from Ref. 20, $x = 0.25$ from Ref. 20, $x = 0.27$ cited from Ref. 17, $x = 0.3$ based on present work, $x = 0.32$ cited from Ref. 22, and $x = 0.33$ cited from Refs. 23 and 24.

TABLE I. Parameters characterizing some Mn perovskites $La_{1-x}A_xMnO_3$ [disorder-corrected $T_C(\langle r_A \rangle, 0)$ are available only near optimal doping (Ref. [25])].

	x	$\langle r_A \rangle$ (Å)	Tolerance factor (t)	σ (Å)	T_C (K)	$T_C(\langle r_A \rangle, 0)$ (K)	GP
Ba	0.1	1.2414	0.92899	0.0762	200		Yes
($T_G \approx 340$ K)	0.12	1.2465	0.93079	0.0825	200		Yes
	0.15	1.2541	0.93347	0.0907	215		Yes
	0.2	1.2668	0.93793	0.1016	251		Yes
	0.27	1.2846	0.94419	0.1128	245	523	Yes
	0.3	1.2922	0.94687	0.2997	310	528	Yes
Ca	0.2	1.2088	0.92337	0.0144	179		No
($T_G \approx 210-255$ K)	0.21	1.2084	0.91741	0.0147	182		Yes
	0.25	1.2072	0.91688	0.0156	200		Yes
	0.27	1.2063	0.91665	0.0159	256	275	Yes
	0.3	1.2051	0.91627	0.0165	206	269	Yes
Sr	0.05	1.2207	0.92172	0.0205	120		No
($T_G \approx 270$ K)	0.08	1.2235	0.92271	0.0255	140		Yes
	0.1	1.2254	0.92337	0.0282	160		Yes
	0.12	1.2273	0.92403	0.0306	180		Yes
	0.15	1.2301	0.92502	0.0336	210		Yes
	0.2	1.2348	0.92668	0.0376	310		No
	0.3	1.2443	0.92991	0.0485	351	439	No

nent λ with composition. The earlier suggestion[17] that this might reflect the fact that the average A site $\langle r_A \rangle$ in this Ba-substituted system near optimal doping is closest to that of the undistorted cubic perovskite structure (r_A^0) (Refs. [25] and [26]) appears to reproduce general trends at this doping level. Specifically that the disorder-corrected T_C—and by inference, T_G—is highest for optimally doped Ba compared to its Ca- or Sr-doped counterparts. However, the broader assertion that $r_A^0 - \langle r_A \rangle$ provides the appropriate criterion for measuring the "disorder" that underlies the tendency to nucleate a Griffiths phase, and the parameters that characterize it, is ruled out by detailed comparisons of the present data with that at $x=0.27$ (Ref. [17]) and with recent data on the Ca-doped system near the ferromagnetic metal-ferromagnetic insulator (FM-FI) boundary.[4] Indeed, an inspection of the various structurally based parameters[3,4,11,13,17–24,27,28] for these systems reproduced in Table I reveals that not a single such parameter reflects the detailed variations in these temperatures, the exponent λ, and the accompanying field dependence of GP behavior, outlined above, away from optimal doping.

Previous studies[4,29] of Ca-doped single crystals, however, revealed that an anomalous behavior of the acoustic spin-wave stiffness D might be a precursor signal for the onset of a Griffiths phase, at least near the FM-FI boundary at $x=0.19$ in that system. The corresponding results for Ba-doped samples provide an interesting comparison. The usual assumptions regarding the dispersion relation for gapless low-lying acoustic mode spin-wave excitations, $\hbar\omega_{ac} = D(T)q^2$, leads to the well-known $T^{3/2}$ expression for the temperature dependence of the spontaneous magnetization[30,31]—viz.,

$$\frac{M_s(T)}{M_S(0)} = 1 - \frac{1}{NS}\left(\frac{k_B T}{4\pi D(T)}\right)^{3/2} \xi\left(\frac{3}{2}\right) \tag{6}$$

in which ξ is the Riemann-zeta function. Figure 6 shows a least-squares fit of Eq. (6) to data below 80 K on the $x=0.3$ single crystal (the spontaneous magnetization being estimated from extrapolation of both Arrott-Noakes and conventional Arrott plots, either being equally applicable well

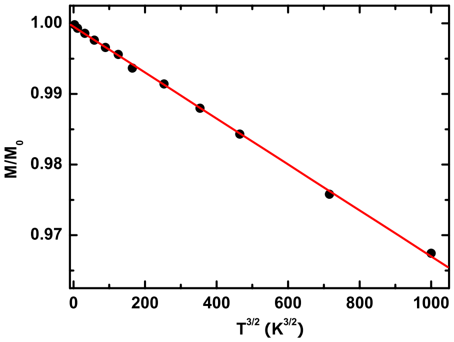

FIG. 6. (Color online) The low-temperature spontaneous magnetization M/M_0, plotted against $T^{3/2}$. The slope of this plot yields a value for the acoustic spin-wave stiffness of $D=147 \pm 2$ meV Å^2.

away from the critical region[32]). This fit yields $D(0) = 147 \pm 2$ meV Å^2, a value in excellent agreement with that reported for a Ba-doped $x = 0.3$ polycrystalline sample $[D(0) = 152 \pm 3$ meV Å$^2]$.[33] More importantly this value for D is well above that reported at $x = 0.27$ $[D(0) = 66 \pm 3$ meV Å^2 (Ref. 31)] (the unusual behavior of the gap parameter at that composition notwithstanding). A rapid decline in the value of D in the Ca-based system coincided with the termination of Griffiths phase characteristics and the occurrence of critical behavior described by Heisenberg model exponents.[4] The parallels with Ba doping are striking; as D declines sharply as x is reduced from 0.3 to 0.27, so do the critical exponents approach very closely to Heisenberg model values. Nevertheless, vestiges of Griffiths phase behavior persist, although they display an extreme sensitivity to field and a much reduced value of the exponent λ (=0.170); correspondingly, the phase regime immediately above T_C at $x = 0.27$ exhibits but minor departures from PM Curie-Weiss behavior. However, whereas in the Ca-doped systems T_C and T_G converge as x is lowered to 0.2, immediately prior to the onset of the FI phase (with antiferromagnetism being established at still lower x values), in the Ba-doped system, Griffiths phase characteristics do not terminate when the composition $x = 0.27$ is approached from either above or below, but persist well below $x = 0.2$ and likely up to optimal doping $x = 0.33$, exhibiting $(T_G - T_C - x)$ boundaries generally similar to LaSrMnO$_3$.[15]

SUMMARY AND CONCLUSIONS

Analysis of magnetic data on single-crystal La$_{0.7}$Ba$_{0.3}$MnO$_3$ yield values for the critical exponents of $\delta = 5.5 \pm 0.3$, $\gamma = 1.41 \pm 0.02$, and $\beta = 0.35 \pm 0.04$, slightly larger than those of the three-dimensional Heisenberg model. Subsequent measurements of the low-field dc and ac susceptibilities reveal features consistent with the presence of a Griffiths phase. These data, combined with previous results, enable a phase diagram of the Griffiths regime for the LaBaMnO$_3$ system in the temperature-composition plane to be constructed, and in connection with the latter, the possible importance of the variation of the acoustic spin-wave stiffness with composition is outlined. Nevertheless, the evolution of Griffiths phase behavior accompanying compositional doping with any specific alkaline-earth cation, as well as the differences displayed using different dopant species, still present considerable challenges to our current understanding of these strongly correlated systems.

ACKNOWLEDGMENTS

Support for this work by the Natural Sciences and Engineering Research Council (NSERC) of Canada is gratefully acknowledged.

---

*jiang@physics.umanitoba.ca

[1] C. Zener, Phys. Rev. **81**, 440 (1950).

[2] A. Moreo, S. Yunoki, and E. Dagotto, Science **283**, 2034 (1999).

[3] M. B. Salamon, P. Lin, and S. H. Chun, Phys. Rev. Lett. **88**, 197203 (2002); M. B. Salamon and S. H. Chun, Phys. Rev. B **68**, 014411 (2003); Pak Yuen Chan, N. Goldenfeld, and M. B. Salamon, Phys. Rev. Lett. **97**, 137201 (2006).

[4] Wanjun Jiang, X. Z. Zhou, G. Williams, Y. Mukovskii, and K. Glazyrin, Phys. Rev. Lett. **99**, 177203 (2007).

[5] *Colossal Magneto-resistive Oxides*, edited by Y. Tokura (Gordon and Breach, Amsterdam, 2000); J. M. D. Coey, M. Viret, and S. V. Molnar, Adv. Phys. **48**, 167 (1999); E. Dagotto, *Phase Separation and Colossal Magnetoresistance* (Springer, Berlin, 2002).

[6] D. Shulyatev, N. Kozlovskaya, R. Privezentsev, A. Pestun, Ya. Mukovskii, L. Elochina, and S. Zverkov, J. Cryst. Growth **291**, 262 (2006).

[7] H. E. Stanley, *Introduction to Phase Transitions and Critical Phenomena* (Clarendon, Oxford, 1971); G. Williams, J. Alloys Compd. **326**, 36 (2001).

[8] J. H. Zhao, H. P. Kunkel, X. Z. Zhou, G. Williams, and M. A. Subramanian, Phys. Rev. Lett. **83**, 219 (1999); Wei Li, H. P. Kunkel, X. Z. Zhou, G. Williams, Y. Mukovskii, and D. Shulyatev, Phys. Rev. B **75**, 012406 (2007).

[9] W. Li, H. P. Kunkel, X. Z. Zhou, G. Williams, Y. Mukovskii, and D. Shulyatev, Phys. Rev. B **70**, 214413 (2004).

[10] D. Kim, B. Revaz, B. L. Zink, F. Hellman, J. J. Rhyne, and J. F. Mitchell, Phys. Rev. Lett. **89**, 227202 (2002).

[11] K. Ghosh, C. J. Lobb, R. L. Greene, S. G. Karabashev, D. A. Shulyatev, A. A. Arsenov, and Y. Mukovskii, Phys. Rev. Lett. **81**, 4740 (1998).

[12] V. Laukhin, B. Martínez, J. Fontcuberta, and Y. M. Mukovskii, Phys. Rev. B **63**, 214417 (2001).

[13] M. Campostrini, M. Hasenbusch, A. Pelissetto, P. Rossi, and E. Vicari, Phys. Rev. B **65**, 144520 (2002).

[14] R. B. Griffiths, Phys. Rev. Lett. **23**, 17 (1969); A. J. Bray, *ibid.* **59**, 586 (1987); A. H. Castro Neto, G. Castilla, and B. A. Jones, *ibid.* **81**, 3531 (1998).

[15] J. Deisenhofer, D. Braak, H.-A. Krug von Nidda, J. Hemberger, R. M. Eremina, V. A. Ivanshin, A. M. Balbashov, G. Jug, A. Loidl, T. Kimura, and Y. Tokura, Phys. Rev. Lett. **95**, 257202 (2005).

[16] C. Magen, P. A. Algarabel, L. Morellon, J. P. Araújo, C. Ritter, M. R. Ibarra, A. M. Pereira, and J. B. Sousa, Phys. Rev. Lett. **96**, 167201 (2006).

[17] Wanjun Jiang, X. Z. Zhou, G. Williams, Y. Mukovskii, and K. Glazyrin, Phys. Rev. B **76**, 092404 (2007).

[18] R. M. Eremina, I. V. Yatsyk, Ya. M. Mukovskii, H.-A. Krug von Nidda, and A. Loidl, JETP Lett. **85**, 51 (2007); I. V. Yatsyk, R. M. Eremina, Ya. M. Mukovskii, H.-A. Krug von Nidda, and A. Loidl, Proceedings of the International Conference on Modern Development of Magnetic Resonance, Kazan, Russian Federation, 2007.

[19] R. Laiho, K. G. Lisunov, E. Lähderanta, M. A. Shakhov, V. N. Stamov, V. S. Zakhvalinskii, V. L. Kozhevnikov, I. A. Leonidov, E. B. Mitberg, and M. V. Patrakeev, J. Phys.: Condens. Matter **17**, 3429 (2005).

[20] P. Mandal and B. Ghosh, Phys. Rev. B **68**, 014422 (2003).
[21] R. I. Zainullina, N. G. Bebenin, A. M. Burkhanov, V. V. Ustinov, and Ya. M. Mukovskii, J. Alloys Compd. **394**, 39 (2005).
[22] S. N. Barilo, G. L. Bychkov, L. A. Kurnevich, S. V. Shiryaev, L. A. Kurochkin, J. W. Lynn, and L. Vasiliu-Doloc, J. Cryst. Growth **211**, 480 (2000).
[23] N. Moutis, I. Panagiotopoulos, M. Pissas, and D. Niarchos, Phys. Rev. B **59**, 1129 (1999).
[24] H. L. Ju, J. Gopalakrishnan, J. L. Peng, Qi Li, G. C. Xiong, T. Venkatesan, and R. L. Greene, Phys. Rev. B **51**, 6143 (1995).
[25] L. M. Rodriguez-Martinez and J. P. Attfield, Phys. Rev. B **54**, R15622 (1996).
[26] N. Rama, M. S. Ramachandra Rao, V. Sankaranarayanan, P. Majewski, S. Gepraegs, M. Opel, and R. Gross, Phys. Rev. B **70**, 224424 (2004).
[27] B. I. Belevtsev, G. A. Zvyagina, K. R. Zhekov, I. G. Kolobov, E. Yu. Beliayev, A. S. Panfilov, N. N. Galtsov, A. I. Prokhvatilov, and J. Fink-Finowicki, Phys. Rev. B **74**, 054427 (2006).
[28] Li, Wei, H. P. Kunkel, X. Z. Zhou, G. Williams, Y. Mukovskii, and D. Shulyatev, J. Phys.: Condens. Matter **16**, L109 (2004).
[29] T. Okuda, Y. Tomioka, A. Asamitsu, and Y. Tokura, Phys. Rev. B **61**, 8009 (2000).
[30] F. Keffer, *Spin Waves, Handbuch der Physik*, Vol. VIII/2 (Springer, Berlin, 1966).
[31] T. Brown, Wei Li, H. P. Kunkel, X. Z. Zhou, G. Williams, Y. Mukovskii, and A. Arsenov, J. Phys.: Condens. Matter **17**, 5997 (2005).
[32] A. Arrott and J. E. Noakes, Phys. Rev. Lett. **19**, 786 (1967); A. Arrott, Phys. Rev. **108**, 1394 (1957).
[33] Tapan Chatterji, L. P. Regnault, and W. Schmidt, Phys. Rev. B **66**, 214408 (2002).